Enhanced Emission of Nile Red Fluorescent Nanoparticles Embedded in Hybrid Sol−Gel Glasses

Maria L. Ferrer and Francisco del Monte*

Instituto de Ciencia de Materiales de Madrid (ICMM), Consejo Superior de Investigaciones Científicas (CSIC), Cantoblanco, 28049 Madrid, Spain

Received: June 7, 2004; In Final Form: September 20, 2004

Highly fluorescent Nile Red (NR) nanoparticles embedded in a hybrid sol−gel glass are reported. The crystallite growth within the confined system created by the porous hybrid matrix results in NR nanoparticles of averaged dimensions below 36 nm. The preparation process allows for the control of both the conformation adopted by single NR molecules prior to aggregation (e.g., near planar) and the configuration of the aggregates (e.g., *oblique* with $\phi < 54.7°$) prior to their assembly in the supramolecular architecture which ultimately forms the nanoparticles. The full preservation of the fluorescent configuration of the aggregates in the nanoparticles is confirmed through the application of the exciton theory, and it is responsible for the significant increase of the fluorescence emission intensity (e.g., up to 525- and 70-fold as compared to that obtained for single NR molecules embedded in pure and hybrid silica glasses, respectively).

Introduction

Most of chromophores show high fluorescence emission in solution at low concentrations ($\sim 10^{-5}-10^{-6}$ M), while the occurrence of intermolecular vibronic interactions leads to a notorious decrease or even the complete vanishing of the fluorescence emission in nondiluted systems.[1] Conjugated organic polymers such as polyphenylenevinylenes and polyphenyleneethynylenes have recently been reported to exhibit high fluorescence in the solid state.[2] Enhanced fluorescence emission in polymers has been ascribed to a synergetic effect of planarization and formation of highly emissive aggregates. The combination of semiconducting properties, high luminescence efficiency, and variability and flexibility in materials synthesis has made highly emissive conjugated polymers the material of choice for a number of applications (e.g., light emitting diodes,[3] light emitting electrochemical cells,[4] and solid-state lasers,[5] among others), which to date were restricted to fluorescent semiconductor or metal nanoparticles.[6]

Organic crystals exhibiting enhanced fluorescence would offer even further variability in the composition and thus in the versatility of many of the attractive applications mentioned above.[7] Highly fluorescent organic nanoparticles have typically been prepared in solution by simple precipitation. The long-term stability and good optical properties of the nanoparticle suspensions have allowed for a complete characterization of their fluorescent properties, which are also ascribed to the above-mentioned synergetic effect of planarization and aggregation. More recently,[8] attention has been given to the control of the aggregate configuration (e.g., H- or J-type) during the crystallization process through, for instance, the selective precipitation in confined systems.[8a,b] Sol−gel host matrixes which are characterized by a uniform porosity could also offer such a confined system.[9] Actually, the sol−gel process has been widely used for the encapsulation of semiconductor nanoparticles (e.g., quantum dots).[10] The nanoparticles are confined within the porous cage of such matrixes which helps to prevent further aggregation and subsequent growth over their quantum size. Since 1984,[11a] the sol−gel process has also been widely used as a method for the encapsulation of organic molecules.[11b,c] More recently, the growth of different organic nanocrystals within the porosity of sol−gel glasses has allowed for the preparation of nanocomposite materials exhibiting nonlinear optical (NLO), magnetic, and fluorescent properties.[12] Nevertheless, further knowledge on the intermolecular arrangement of the aggregates (e.g., H- or J-type) which ultimately form the nanoparticles would be desired in order to optimize their fluorescence response.

Herein, we report on the preparation of highly fluorescent Nile Red (NR) nanoparticles embedded in hybrid sol−gel glasses. The selection of NR embedded in hybrid matrixes as the model system of study was based on the belief that it fits the above-mentioned requirements for the achievement of fluorescence in nanoparticles, that is, the synergetic effect of planarization and formation of highly emissive aggregates. NR is a well-known solvatochromic probe whose planar conformation is highly fluorescent.[13] Hybrid silica matrixes were prepared from glycidoxypropyltrimethoxysilane which favors the fluorescent NR conformation (e.g., planar) versus the nonfluorescent one (e.g., twisted) (Scheme 1).[14] The conformation adopted by NR within the porous cage of the hybrid matrixes was unambiguously determined through fluorescence spectroscopy, time resolved, and anisotropy measurements. NR aggregation was induced by increasing the dye concentration. Control on both the configuration of the NR aggregates (e.g., *oblique*[15]) and the geometry adopted by the monomer constituents in such a configuration (e.g., the angles α and ϕ and the separation distance (R) between the monomer units,[16] Figure 1) ultimately determines the achievement of fluorescent rather than nonfluorescent aggregates embedded in a hybrid sol−gel matrix. The preservation of this geometry in the supramolecular architecture which forms the nanocrystals allows for the unprecedented high fluorescent performance observed in this work for NR nanoparticles.

* Corresponding author. E-mail: delmonte@icmm.csic.es.

10.1021/jp047550u CCC: $30.25
Published on Web 12/16/2004

SCHEME 1: Nonfluorescent Twisted (Left) and Fluorescent Planar (Right) Conformations of NR[a]

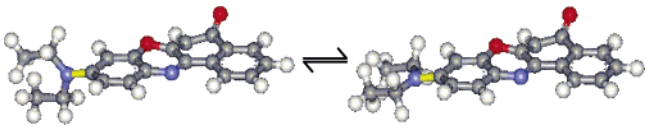

[a] The yellow-marked N−C bond is the rotary bond.

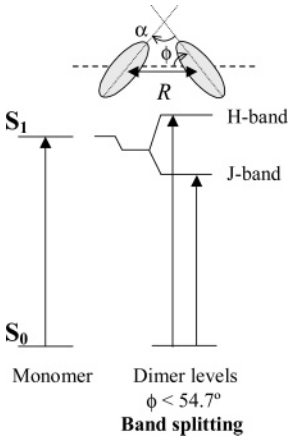

Figure 1. Exciton band energy diagram for aggregates in an *oblique* configuration.

Experimental Section

Single NR molecules (from Aldrich) were dispersed in pure silica glasses (e.g., NRS1) by mixing 9.1 mmol of tetramethyl orthosilicate (TMOS, from Aldrich) and 36.4 mmol of H_2O under vigorous stirring. NR was added to the hydrolyzed sol as a methanol solution, that is, 3×10^{-6} mmol of NR in 33 mmol of methanol (from Merck). Single NR molecules were dispersed in hybrid silica glasses (e.g., NRH1) as described above for NRS1 except that 3.64 mmol of TMOS and 5.46 mmol of glycidoxypropyltrimethoxysilane (GPTMS, from Aldrich) were used as silicon alkoxyde precursors. Increased amounts of NR (3×10^{-5}, 1.5×10^{-4}, 3×10^{-4}, 7.5×10^{-4}, and 1.5×10^{-3} mmol) were used to induce aggregation in the resulting glasses (NRS2−NRH2, NRS3−NRH3, NRS4−NRH4, NRS5−NRH5, and NRS6−NRH6, respectively). In every case, the mixture was stirred for 60 min, then transferred to a polystyrene cuvette, and covered with aluminum foil. After gelation, the aluminum foil was perforated to allow the slow evaporation of the solvents until the formation of xerogels. Xerogels were dried at 50 °C for 10 days prior to the spectroscopic measurements.

Fluorimetric measurements were performed at 25 °C on a 48000s (T-Optics) spectrofluorometer from SLM-Aminco. Emission (excitation wavelength at 475 nm for NRH samples and at 515 nm for NRS samples) and excitation (emission wavelength at 675 nm for NRH samples and at 725 nm for NRS samples) spectra were recorded by reflection (*front face* mode) in backward direction on pills of 50 μm thickness prepared from finely ground samples.[17] Steady-state fluorescence anisotropy was measured on bulk samples with cubic shape and 0.5 cm path lengths, as described elsewhere.[18] Lifetimes were measured by reflection (*front face* mode) in backward direction on finely ground samples packed into quartz cells with 1 mm path lengths, as described elsewhere.[18] Multifrequency phase and modulation fluorescence spectroscopy was used for lifetime measurements.[19] The method provides two determinations of the fluorescence lifetimes from two independent measurements, that is, phase and modulation. Phase and modulation data were collected at 20−25 modulation frequencies averaging 150 readings in order to minimize any uncertainty of the measurements. The frequency dependent phase and modulation data were analyzed using a nonlinear least-squares procedure that minimizes the squared deviations between the observed and the expected phase and modulation values. The values of the floating parameters (lifetimes and fractional intensities of every fluorescent species contributing to the total fluorescence intensity) are varied in a direction that minimizes the value of the deviations between the model and the data χ^2_R (the reduced error). Computation is finished with a number of iterations through the fitting algorithm, when a minimum is found. Values of χ^2_R greater than unity may indicate either the presence of systematic errors or an inappropriate mode.[20] An uncertainty of 0.5 to the resolution of the phase and 0.005 to the resolution of the modulation was applied for the calculation of χ^2_R. The accuracy of the lifetime values measured was determined according to the lower χ^2_R value found in each individual measurement.[21] The best χ^2_R values were always obtained for data fitted to a single component rather than to more than one component, which means that the total fluorescence intensity results from just one fluorescent species.[21]

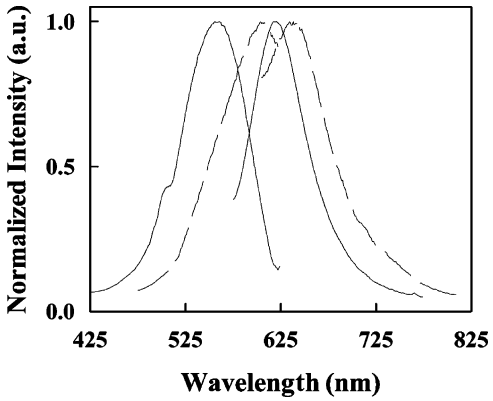

Figure 2. Normalized excitation and emission spectra of NRS1 (dashed line) and NRH1 (solid line).

The rotational reorientation kinetics were obtained from the frequency-domain anisotropy decays.[22] Measurements were achieved in *right angle* mode on bulk samples with cubic shape and 0.5 cm path lengths.[18,23] The frequency dependent phase data were analyzed using a nonlinear least-squares procedure evaluated over different models, as described elsewhere.[18] The experimental lifetimes were introduced as fixed parameters in each of the analyzed models. The accuracy of the anisotropy measurements was based on the best χ^2_R values obtained after the fitting of the data, as described above for lifetimes.

Ultraviolet−visible (UV−vis) spectroscopy was performed at 25 °C on a Varian model 2300 UV−vis spectrophotometer. The absorption spectra of NRS1−NRS6 and NRH1−NRH6 were measured in reflectance mode on samples finely ground and packed in quartz cells with 1 mm path lengths. The extinction coefficient of NRH1 was measured in transmittance mode on a bulk sample with a 3 mm path length ($\int \epsilon(\nu)\, d\nu = 1.19 \times 10^8\ M^{-1}\ cm^{-1}$).

Scanning electron microscopy (SEM) was performed on a Zeiss DSM-950 instrument.

Infrared spectra were recorded on a Nicolet model 20SXC Fourier transform infrared (FT-IR) spectrophotometer on KBr pills prepared with fine powder of the samples.

Results and Discussion

The emission and excitation spectra for low loadings of NR encapsulated in a pure silica and in a hybrid glass (NRS1 and

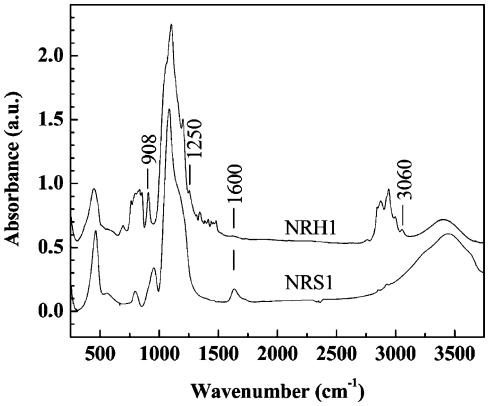

Figure 3. FT-IR spectra of NRS1 and NRH1.

TABLE 1: Maximum of Excitation (λ_{mex})[a] and Emission (λ_{mem})[b] Spectra, Lifetimes (τ),[b] and Experimental Reduced Chi-Squared (χ^2_R) Values for NRH1−NRH6[c] and the Calculated ϕ Angle for NRH3−NRH6

	λ_{mex} (nm)	λ_{mem} (nm)	τ (ns)	χ^2_R	ϕ (deg)
NRH1	560	619	4.00 ± 0.15	1.1	monomer
NRH2	560	622	4.45 ± 0.15	1.0	
NRH3	506−561	624	4.60 ± 0.15	1.0	48.7 ± 0.8
NRH4	504−562	628	4.83 ± 0.15	0.9	49.9 ± 0.8
NRH5	503−563	633	4.85 ± 0.15	1.2	50.0 ± 0.8
NRH6	503−564	634	4.86 ± 0.15	1.1	50.1 ± 0.8

[a] The emission wavelength used to record the excitation spectra was 675 nm. [b] The excitation wavelength used to record the emission spectra and to measure the lifetime values was 475 nm. [c] Errors were calculated as described elsewhere.[20,21]

NRH1, respectively) are shown in Figure 2. The excitation-spectra of both NRS1 and NRH1 reveal the absence of nonaggregated species. However, large differences in both the position of the excitation and emission peaks and the fluorescence efficiency of NRS and NRH samples can be observed. It is well-known that protic environments favor the nonfluorescent twisted conformation of NR, while nonprotic environments favor its highly fluorescent planar conformation.[13] Besides the purple color of the NRS1 sample, the position of its emission maximum (638 nm) and its poor fluorescence efficiency are characteristic for NR in a protic environment such as that created by the Si−OH groups of silica glasses. Meanwhile, the magenta color of the NRH1 sample, the position of its emission maximum (619 nm), and its large fluorescence efficiency (up to 7.5-fold as compared to NRS1) are characteristic for NR in a homogeneous nonprotic environment such as that created by the glycidoxypropyl groups of hybrid glasses.[14] Note that, under the experimental conditions used in this work, the glycidoxypropyl groups do not get converted into protic alcohol groups.[14,24] The FT-IR spectrum of NRH1 shown in Figure 3 corroborates the presence of the epoxy group (e.g., bands at 3060, 1250, and 908 cm^{-1}).[14,24] The absence of main band characteristic of water (observed in NRS1 at around 1600 cm^{-1}) indicates the lack of remaining solvents (e.g., not only water but also methanol, since its boiling point is below that of water) from the preparation process. Nevertheless, the homogeneity of the environment surrounding NR at the porous cage of the NRH1 sample is confirmed below through lifetime and anisotropy measurements (both steady-state and time resolved fluorescence anisotropy).

The analysis of the frequency dependent phase and modulation data allows the determination of a single fluorescent lifetime for NRH1 (Table 1), which resembles the homogeneity of the NR surrounding environment. Otherwise, more than one lifetime value would be obtained.[25] The measured lifetime value (4.0 ns) is also in concordance with NR adopting a planar conformation; that is, hindrance rotation of the amine groups minimizes the deactivation processes or quenching ($S_1 \rightarrow S_0$ internal conversion processes), giving rise to lifetime values within the 3−4 ns range.[26]

TABLE 2: Experimental ($\langle r \rangle$) and Calculated ($\langle r \rangle$*) Steady-State Fluorescence Anisotropy of NRH1. Initial anisotropy (r_0), rotational correlation times (Φ), and residual anisotropy (r_∞) were recovered at 20 °C from time resolved anisotropy analyzed according to the hindered rotator model up to reach the best chi-squared (χ^2_R) values. The local microviscosity (η) is also included

$\langle r \rangle$	$\langle r \rangle$*	r_0	r_∞	Φ (ns)	χ^2_R	η (cP)
0.275	0.278	0.340	0.203	4.87	0.65	86

Meanwhile, the $\langle r \rangle$ value recovered from the steady-state anisotropy measurement of NRH1 was below that expected for a vitrified system but high enough to indicate a slowed or partially hindered dynamic (Table 2).[27] Nevertheless, steady-state anisotropy measurements just provide insight into the average environment about the fluorescent probe. Time resolved anisotropy provides the underlying rotational motions and allows for an estimation of the local microviscosities at the dye surrounding environment. The experimental data were modeled as a hindered rotator (eq 1),[28] which is the model employed for dyes trapped in confined systems such as polymers, micelles, sol−gel glasses, and ormosils.[17,22,29]

$$r(t) = [(r_0 - r_\infty) \exp(-t/\Phi)] + r_\infty \quad (1)$$

where r_0 is the fundamental anisotropy, r_∞ is the residual anisotropy which is related to the cone angle of the wobbling, and Φ is the apparent orientational relaxation time (Table 2). In this model, the apparent relaxation time (Φ) is given by

$$\Phi = \frac{\sigma}{D_W} \quad (2)$$

where D_W is the wobbling diffusion constant and σ is a constant that solely depends on the value of r_0/r_∞, that is, the angle of wobbling.[28b] The goodness of the fitting of the experimental data found for NRH1 to the spatially hindered rotator model was reflected not only by the low chi-squared value but also by the good agreement between the measured and calculated $\langle r \rangle$ values (Table 2).[29c]

The average value of the recovered fundamental anisotropy (r_0, in Table 2) was close to the predicted fundamental anisotropy for a probe with a high symmetry.[27] Moreover, nonzero anisotropy (r_∞, in Table 2) values were observed, which as mentioned above is characteristic of confined systems.[28] This value contains implicitly information about the order of the environment, reflecting the degree of orientational constraint due to the surrounding media, that is, the higher the r_∞ values, the stronger the orientational constrain of the fluorescent probe. Thus, the high r_∞ value observed in NRH1 is indicative of NR in a restricted orientational domain.

The experimental D_W value can be obtained from eqs 2 and 3, and it is possible to estimate the local microviscosity (η) sensed by the probe using a modified form of the Stokes−Einstein−Debye (SED) theory:[22]

$$D_W = \frac{kT}{6\eta f V_{eff}} \quad (3)$$

where k is the Boltzmann constant, T is the temperature, V_{eff} is the effective volume, that includes the Perrin shape factor which

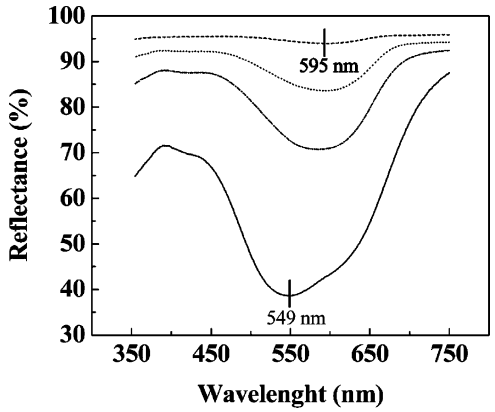

Figure 4. Reflectance spectra of NRS1 (dotted line), NRS2 (dashed line), NRS3 (dash−dotted line), and NRS6 (solid line).

takes into account the asymmetry of the rotating object, and f is a dimensionless factor that depends on the friction mechanism ($f = 1$, for stick boundary conditions). The contribution of the dielectric friction in eq 3 is omitted, since, as reported elsewhere,[30] it is negligible for NR in polar nonprotic solvents.

The bowling diffusion constant value (σ) is obtained from eq 4 through the polynomial approximation of the data as a function of the experimentally determined r_∞/r_0 values:[28a,b]

$$\sigma = 0.1674 - 0.106\,61(r_\infty/r_0) - 0.062(r_\infty/r_0)^2 \qquad (4)$$

Taking into account that the van der Waals volume of NR is 285 Å^3 and the molecular shape of NR is a prolate ellipsoid (the shape factor is 1.64), the effective volume of the resulting revolution ellipsoid can be calculated as described elsewhere ($V_{\text{eff}} = 467$ Å^3).[31] In NRH1, eq 3 gives a local "apparent" microviscosity at a NR surrounding environment of 86 cP. Time resolved anisotropy measurements were also attempted on NRS1, but the above-mentioned poor fluorescence efficiency of this sample impeded the achievement of reliable data. In any case, fluorescence anisotropy[18b] and nuclear magnetic resonance (NMR) experiments[32] performed on dyes allocated at the hydrated porous surface of sol−gel glasses, hence in close contact with silanol groups, have provided microviscosity values 1 order of magnitude lower (e.g., 4−5 cP). The high microviscosity value obtained in our case is therefore indicating that NR is homogeneously surrounded by the organic moieties at the porous cage of ormosils,[18,29d] and far from the silanol groups of the porous surface.

NR aggregation was induced by the concentration increase of the entrapped dye. The absorption spectrum of the aggregates consists of two separate bands (J- and H-bands, in Figure 1), being the aggregate geometry reflected in the relative intensity of these bands;[16] for example, the H-band is always stronger than the J-band in the *parallel plane twist angle* model (e.g., *sandwich*-type aggregates) while the opposite relation takes place in the *in-plane oblique angle* model (e.g., *oblique* aggregates). The occurrence of band splitting in the reflectance spectra of NRS2−NRS6 with a strong H-band placed at 549 nm (Figure 4) besides the lack of changes in the NRS2−NRS6 excitation spectra as compared to that shown for NRS1 in Figure 2 indicates that the concentration increase in NRS samples results in the formation of *sandwich*-type aggregates which are nonfluorescent. Quenching of the fluorescence occurs in this geometry as a consequence of the strong intermolecular interactions arising from planar π-conjugated chromophores.[33] Actually, the fluorescence intensity of NRS2−NRS6 samples is negligible (Figure 5). In regard to NRH samples, the linear plot

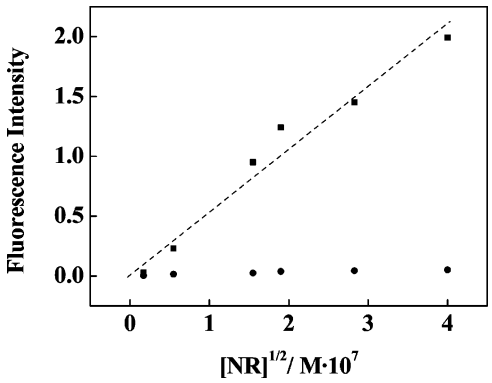

Figure 5. Plot of the absolute fluorescence intensity of NRS1−NRS6 (●) and NRH1−NRH6 (■) versus the square root of the NR concentration.

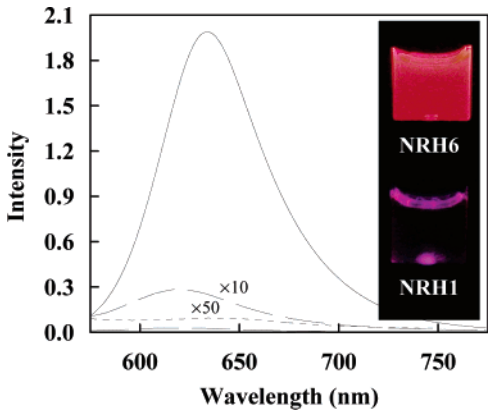

Figure 6. Absolute emission spectra of NRS1 (dotted line), NRH1 (dashed line), and NRH6 (solid line). Note that the emission spectra of NRS1 and NRH1 are magnified (×50 and ×10, respectively) for better comparison. Inset: photograph of the fluorescence emitted by NRH1 and NRH6 under UV irradiance. The bulk thickness is ∼3.0 mm.

found for the fluorescence intensity with the square root of the dye concentration all over the studied range of concentrations (NRH1−NRH6) indicates the formation of fluorescent aggregates (Figure 5).[34] Moreover, the increase of the fluorescence intensity is remarkable, for example, up to 525-fold as compared to NRS samples and more than 70-fold as compared to NRH1 (Figures 5 and 6). The emission spectra are red shifted from NRH1 to NRH6 (Table 1), reflecting an increase of the polarizability at the dye surrounding environment. Such an increase of the polarizability must be explained in terms of the close packaging of dye moieties in the aggregates,[33] given that there are no further changes at the NR surrounding environment of the different samples. Lifetime measurements also corroborate both the fluorescent character of the aggregates and the homogeneity of their surrounding environment. The former, since otherwise, the formation of nonfluorescent aggregates would contribute to the quenching of the excited states through intersystem crossing processes.[35] The latter, since as mentioned above, the best fit of data is always obtained for a monoexponential model rather than for a bi- or a triexponential model.[25]

The excitation spectra of NRH2−NRH6 (Figure 7) with a J-band more intense than the H-band are characteristic of aggregates in an *in-plane oblique angle* configuration. The geometry of *oblique* aggregates is basically defined by the chromophore spacing (R) and the relative spatial arrangement of the transition dipole moments of the molecules (ϕ and α) forming the aggregates (Figure 1). The achievement of fluorescence in aggregates adopting an *oblique* configuration also

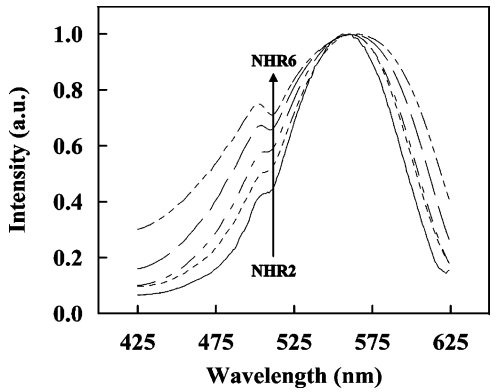

Figure 7. Normalized excitation spectra of NRH2−NRH6.

has some geometric requirements; that is, the ϕ angle values must be in the 0−54.7° range.[15] Structural information on the aggregates regarding the simplest geometry model can experimentally be obtained through the application of the exciton theory.[15,16,36] Thus, the ϕ angle can be obtained through eq 5 from the radiative rate constant of the fluorescent aggregates (k_{r_D}) and of the monomer unit (k_{r_M}):[15]

$$k_{r_D} = 2k_{r_M} \cos^2 \phi \tag{5}$$

As described above, the main mechanism of nonradiative deactivation (e.g., rotation about the xanthene−amine bond) is minimized in NRH samples. Under these circumstances, the radiative rate constant of both the monomer and the fluorescent aggregates can directly be approximated to the inverse of the lifetime values of NRH1 and NRH3−NRH6, respectively.[37] The values of the α angles obtained below will also confirm the validity of such an approximation; that is, note that the sum of α plus 2ϕ is ∼180° (Figure 1). Thus, the calculated ϕ angles for NRH3−NRH6 samples are reported in Table 1 and confirm the fluorescent character of the aggregates, that is, ϕ < 54.7°.[15] Actually, the fluorescent character of the aggregates could have already been inferred from their capability to be observed in the excitation spectra.

At this stage, the authors want to mention that a distribution of aggregate geometries rather than abrupt changes in the geometry would be a more realistic picture of the situation resulting from the gradual increase of the dye concentration. Nevertheless, the presence of very different species within such a distribution (e.g., from nonaggregates to aggregates) can be disregarded, since the accuracy of the measurement is good enough to discriminate their lifetimes (4.0 ns and in the 4.6−4.9 ns range, respectively).[20]

The application of the exciton theory on the excitation spectra of the fluorescent aggregates allows for the complete characterization of their structure (α and *R*, in Figure 1).[38] The α angle is calculated from the ratio between the areas of the long-wavelength (A_1) and short-wavelength (A_2) excitation bands (eq 6). The interaction energy (*U*, in cm^{-1}) between the monomers forming the aggregate is calculated from the long-wavenumber (ν_2, in cm^{-1}) and short-wavenumber (ν_1, in cm^{-1}) excitation bands (eq 7).

$$\tan^2(\alpha/2) = A_1/A_2 \tag{6}$$

$$U = (\nu_2 - \nu_1)/2 \tag{7}$$

The goodness of the calculated data is corroborated by the sum α + 2ϕ = 180° (Figure 1). The α value obtained for NR

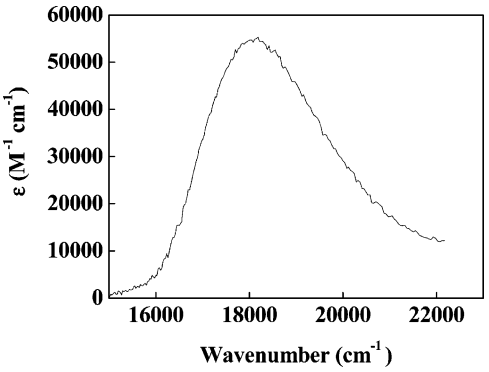

Figure 8. Plot of NRH1 extinction coefficient versus wavenumber ($\int \epsilon(\nu)\, d\nu = 1.19 \times 10^8$ M^{-1} cm^{-1}).

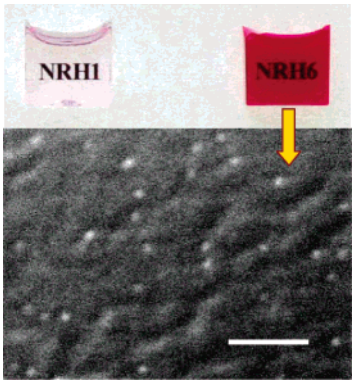

Figure 9. (bottom) SEM micrograph of NR nanoparticles in NRH6 (the bar is 150 nm). (top) Photograph of transparent NRH1 and NRH6 bulk samples (the bulk thickness is ∼3.0 mm).

chromophores in the nanoparticles (e.g., ∼80.5° for NRH6) resembles a geometry close to that reported as the most efficient configuration in condensed media to prevent any decrease in luminescence efficiency, that is, long axes perpendicular in adjacent chromophores.[39]

For the *oblique* configuration, the separation distance between the molecules (*R*, in angstroms) can be obtained from eq 8

$$R = \left(\frac{1.85 \times 10^2 \int \epsilon(\nu)\, d\nu\, [\cos(\alpha) + 3 \sin(\alpha/2)]}{U \nu_m} \right)^{1/3} \tag{8}$$

where ν_m (in cm^{-1}) and $\int \epsilon(\nu)\, d\nu$ (in M^{-1} cm^{-1}) are the wavenumber at the maximum intensity and the area of the absorption band of NRH1, respectively (Figure 8). The experimental values of the intermolecular distance (*R*) found for NRH3−NRH6 are in range to those reported for *oblique* aggregates formed from dyes with similar molecular structures (e.g., xanthene-like molecules).[36,38]

It is worth noting the tendency of α and *R* values in the range of the studied NR concentrations. In a first stage, α decreases from 85° for NRH3 to 80° for NRH4, indicating some rearrangement of the chromophores with the increase of concentration.[38] From NRH4 to NRH6, α remains constant (∼80°) within the experimental error. The tendency of *R* is equivalent to that observed for α; that is, *R* decreases from 12.1 Å for NRH3 to 10.7 Å for NRH4, and from then on (NRH4−NRH6), it keeps a similar value.

The SEM micrograph of NRH6 reveals the presence of monodisperse NR nanoparticles dispersed within the hybrid matrix (Figure 9, bottom). The particle size in the nanometer range (∼36 nm) allows for the excellent optical transparency of the sample (Figure 9, top). The invariance of α and *R* values

observed for NRH4−NRH6 samples must be in relation to the crystallite formation. The classical model for nanocrystal formation is nucleation and growth.[40] Nucleation occurs when a critical concentration value (e.g., supersaturation) is reached. After nucleation, concentration falls momentarily below the critical threshold so that no new nuclei are formed and the incorporation of the remaining active molecules results in the growth of the existing nuclei. If it is possible to set high values of supersaturation, nanoparticle formation can also occur by a diffusion limited aggregation mechanism with active participation of suitable active molecules.[41] The elucidation of the formation mechanism of the fluorescent nanoparticles is not an easy issue, as pointed out in a recent review on the subject.[40] Nevertheless, it is well-known that the nanoparticle formation process influences its fluorescent character.[8] Actually, the process previously described for the formation of nonfluorescent nanoparticles in sol−gel matrixes shows two clear differences compared with the preparation process followed in this work; first, the nature of the fluid medium in which nucleation and crystallization occur, and second and principal, the formation of first nuclei from nonaggregated molecules when the temperature is changed from 80 to 25 °C.[12] The above-mentioned decrease of the concentration after nucleation avoids the formation of new nuclei, and subsequent solvent evaporation at the gel state just promotes the grow of the nuclei. In our case, the process runs without drastic temperature changes and the progressive increase of the NR concentration during drying of the gels first results in the formation of disperse aggregates, which become crystals when the NR concentration reaches the critical concentration value.[40] The experimental results indicate that the critical concentration value of NR in NRH matrixes eventually corresponds to that of NRH4. Above the NRH4 concentration (e.g., NRH5−NRH6), fluorescent aggregates incorporate to the crystalline structure contributing to the growth of the nanocrystals.[41] The experimentally observed preservation of the fluorescent aggregate geometry in the supramolecular architecture which ultimately forms the nanoparticles would corroborate the proposed mechanism of nanoparticle formation based on aggregation. Otherwise, rearrangement of the chromophores would result in the vanishing of the fluorescence.[8c,d]

Conclusions

In summary, we have demonstrated that if one desires to obtain highly fluorescent NR nanoparticles encapsulated in sol−gel matrixes, control of both the conformation adopted by single NR molecules prior to aggregation (e.g., near planar) and the configuration of the J-aggregates (e.g., *oblique* with $\phi > 54.7°$) prior to their assembly in the supramolecular architecture which ultimately forms the nanoparticles is required. The nanoparticle formation process described above is in good concordance to that described for fluorescent nanoparticles in solution, that is, a synergetic effect of planarization and formation of highly emissive aggregates. NR in its near planar conformation is obtained through the allocation of NR in close contact with the organic moieties of the porous cage of the hybrid matrixes, as revealed by fluorescence spectroscopy, time resolved, and anisotropy measurements. Moreover, the formation of the nanocrystals with a defined lattice cell where the positions and distance of single molecules resemble those of the fluorescent aggregates in the *oblique* configuration (e.g., $\phi < 54.7°$) is crucial for the achievement of highly fluorescent NR nanoparticles. All these features make these sol−gel nanocomposites of great interest for the development of optical applications to date restricted to materials such as fluorescent polymers and fluorescent semiconductor or metal nanoparticles.

Acknowledgment. M.L.F. is grateful to MCYT for a *Ramon y Cajal* research contract. This work was supported by the CICYT-MAT2003-02718 and CSIC-PIF200460F027 projects.

References and Notes

(1) Birks, J. B. *Photophysics of Aromatic Molecules*; Wiley: London, 1970.

(2) (a) Deans, R.; Kim, J.; Machacek, M. R.; Swager, T. M. *J. Am. Chem. Soc.* **2000**, *122*, 8565−8566. (b) Levitus, M.; Schmieder, K.; Ricks, H.; Shimizy, K. D.; Bunz, U. H. F.; Garcia-Garibay, M. A. *J. Am. Chem. Soc.* **2001**, *123*, 4259−4265.

(3) (a) Burroughes, J. H.; Bradley, D. D. C.; Brown, A. R.; Marks, R. N.; Friend, R. H.; Burn, P. L.; Holmes, A. B. *Nature* **1990**, *347*, 530. (b) Ho, P. K. H.; Thomas, D. S.; Friend, R. H.; Tessler, N. *Science* **1999**, *285*, 233.

(4) Pei, Q.; Yu, C.; Zhang, Y.; Yan, Y.; Heeger, A. J. *Science* **1995**, *268*, 1086.

(5) Hide, F.; Diaz-Garcia, M. A.; Schwartz, B.; Andersson, M. R.; Pei, Q.; Heeger, A. J. *Science* **1996**, *273*, 833. (b) Tessler, N.; Denton, G. J.; Friend, R. H. *Nature* **1996**, *382*, 695.

(6) Alivisatos, A. P. *Science* **1996**, *271*, 933. (b) Ashoori, R. C. *Nature* **1996**, *379*, 413.

(7) (a) Kasai, H.; Kamatani, H.; Yoshikawa, Y.; Okada, S.; Oikawa, H.; Watanabe, A.; Ito, O.; Nakanishi, H. *Chem. Lett.* **1997**, *9*, 1181−1182. (b) Komai, Y.; Kasai, H.; Hirakoso, H.; Hakuta, Y.; Okada, S.; Oikawa, H.; Adschiri, T.; Inomata, H.; Arai, K.; Nakanishi, H. *Mol. Cryst. Liq. Cryst. Sci. Technol., Sect. A* **1998**, *322*, 167−172. (c) Luo, J.; Xie, Z.; Lam, J. W. Y.; Cheng, L.; Chen, H.; Qiu, C.; Kwok, H. S.; Zhan, X.; Liu, Y.; Zhu, D.; Tang, B. Z. *Chem. Commun.* **2001**, 1740−1741. (d) Fu, H.-B.; Yao, J.-H. *J. Am. Chem. Soc.* **2001**, *123*, 1434−1439. (e) An, B.-K.; Kwon, S.-K.; Jung, S.-D.; Park, S. Y. *J. Am. Chem. Soc.* **2002**, *124*, 14410−14415. (f) Würthner, F.; Yao, S.; Beginn, U. *Angew. Chem., Int. Ed.* **2003**, *42*, 3247−3250.

(8) (a) Peyratout, C. S.; Möhwald, H.; Dähne, L. *Adv. Mater.* **2003**, *15*, 1722−1726. (b) Jang, J.; Oh, J. H. *Adv. Mater.* **2003**, *15*, 977−980. (c) Auweter, H.; Haberkorn, H.; Heckmann, W.; Horn, D.; Lüddecke, E.; Rieger, J.; Weiss, H. *Angew. Chem., Int. Ed.* **1999**, *38*, 2188. (d) Li, C.-J.; Zeng, Q.-D.; Liu, Y.-H.; Wan, L.-J.; Wang, C.; Wang, C.-R.; Bai, C.-L. *ChemPhysChem* **2003**, *4*, 857.

(9) Brinker, C. J.; Scherer, G. W. *Sol Gel Science*; Academic Press: San Diego, CA, 1990.

(10) (a) Wu, N.-L.; Wang, S.-Y.; Rusakova, I. A. *Science* **1999**, *285*, 1375−1377. (b) Parala, H.; Winkler, H.; Kolbe, M.; Wohlfart, A.; Fischer, R. A.; Schmechel, R.; von Seggern, H. *Adv. Mater.* **2000**, *12*, 1050−1056.

(11) (a) Avnir, D.; Levy, D.; Reisfeld, R. *J. Phys. Chem.* **1984**, *88*, 5956. (b) Sanchez, C.; Ribot, F. *New J. Chem.* **1994**, *18*, 1007. (c) Minoofar, P. N.; Hernandez, R.; Chia, S.; Dunn, B.; Zink, J. I.; Franville, A.-C. *J. Am. Chem. Soc.* **2002**, *124*, 14388−14396.

(12) (a) Ibanez, A.; Maximov, S.; Guiu, A.; Chaillout, C.; Baldeck, P. L. *Adv. Mater.* **1998**, *10*, 1540−1543. (b) Sanz, N.; Gaillot, A.-C.; Usson, Y.; Baldeck, P. L.; Ibanez, A. *J. Mater. Chem.* **2000**, *10*, 2723−2726. (c) Sanz, N.; Wang, I.; Zaccaro, J.; Beaugnon, E.; Baldeck, P. L.; Ibanez, A. *Adv. Funct. Mater.* **2002**, *12*, 352−358. (d) Botzung-Appert, E.; Monnier, V.; Duong, T. H.; Pansu, R.; Ibanez, A. *Chem. Mater.* **2004**, *16*, 1609−1611 and references therein.

(13) Rettig, W. *Photochemical Processes in Organized Molecular Systems*; North-Holland: New York, 1991; p 61.

(14) Moreno, E. M.; Levy, D. *Chem. Mater.* **2000**, *12*, 2334−2340.

(15) (a) Kemnitz, K.; Yoshihara, K. *J. Phys. Chem.* **1991**, *95*, 6095. (b) Kemnitz, K.; Tamai, N.; Yamazaki, I.; Nakashima, N.; Yoshihara, K. *J. Phys. Chem.* **1986**, *90*, 5094.

(16) (a) Kasha, M.; Rawls, H. R.; El-Bayoumi, M. A. *Pure Appl. Chem.* **1965**, *11*, 371. (b) McRae, E. G.; Kasha, M. *Physical Processes in Radiation Biology*, 1st ed.; Academic Press: New York, 1964. (c) McRae, E. G.; Kasha, M. *J. Chem. Phys.* **1961**, *11*, 38.

(17) Oelkrug, D. *Topics in Fluorescence Spectroscopy: Probe Design and Chemical Sensing*; Lakowicz, J. R., Ed.; Plenum Press: New York, 1994; Vol. 4, Chapter 8.

(18) (a) del Monte, F.; Ferrer, M. L.; Levy, D. *J. Mater. Chem.* **2001**, *11*, 1745. (b) Ferrer, M. L.; del Monte, F.; Levy, D. *J. Phys. Chem. B* **2001**, *105*, 11076.

(19) Lackowicz, J. R.; Laczko, G.; Cherk, H.; Gratton E.; Limkeman, M. *Biophys. J.* **1984**, *46*, 462.

(20) Bevington, P. R. *Data Reduction and Error Analysis for the Physical Sciences*; McGraw-Hill, Inc.: New York, 1969; p 336.

(21) Gratton, E.; Linkeman, M. *Biophys. J.* **1983**, *44*, 315.

(22) (a) Lackowicz, J. R. *Principles of Fluorescence Spectroscopy*; Plenum Press: New York, 1983; Chapter 5. (b) Steiner, R. F. *Topics in Fluorescence Spectroscopy: Probe Design and Chemical Sensing*; Lakowicz, J. R., Ed.; Plenum Press: New York, 1991; Vol. 2, Chapter 1.

(23) (a) Narang, U.; Wang, R.; Prasad, P. N.; Bright, F. V. *J. Phys. Chem.* **1994**, *98*, 17. (b) Soyez, H.; Huang, M.; Dunn, B. S.; Zink, J. I. *Proc. SPIE-Int. Soc. Opt. Eng.* **1997**, *3136*, 118.

(24) Innocenzi, P.; Brusatin, G.; Guglielmi, M.; Bertani, R. *Chem. Mater.* **1999**, *11*, 1672.

(25) Dutta, A. K.; Kamada, K.; Ohta, K. *Chem. Phys. Lett.* **1996**, *258*, 369.

(26) (a) Itho, K.; Honda, K. *Chem. Phys. Lett.* **1982**, *87*, 213. (b) Vogel, M.; Rettig, W.; Sens, R.; Drexhage, K. H. *Chem. Phys. Lett.* **1988**, *147*, 461.

(27) Dale, R. E. *Time Resolved Fluorescence Spectroscopy in Biochemistry and Biology*; Cundall, R. B., Dale R. E., Eds.; NATO ASI Series A: Life Sciences; Plenum Press: New York, 1983; Vol. 69, pp 605−606.

(28) (a) Mateo, C. R.; Souto, A. A.; Amat-Guerri, F.; Acuña, A. U. *Biophys. J.* **1996**, *71*, 2177. (b) Kinoshita, K.; Kawato, S.; Ikegami, A. *Biophys. J.* **1977**, *20*, 289. (c) Lipari, G.; Szabo, A. *Biophys. J.* **1980**, *30*, 489.

(29) (a) Wittouck, N.; Negri, R. M.; Ameloot, M.; De Schryver, F. C. *J. Am. Chem. Soc.* **1994**, *116*, 10601. (b) Dutt, G. B.; Ameloot, M.; Bernik, D.; Negri, R. M.; De Schryver, F. C. *J. Phys. Chem.* **1996**, *100*, 9751. (c) Marchi, M. C.; Bilmes, S. A.; Negri, R. M. *Langmuir* **1997**, *13*, 3665. (d) Baker, G. A.; Jordan, J. D.; Bright, F. V. *J. Sol.-Gel Sci. Technol.* **1998**, *11*, 43.

(30) Vauthey, E. *Chem. Phys. Lett.* **1993**, *216*, 530.

(31) (a) Dutt, G. B.; Doraiswamy, S.; Periasamy, N. *J. Chem. Phys.* **1990**, *93*, 8498. (b) Dutt, G. B.; Doraiswamy, S.; Periasamy, N. *J. Chem. Phys.* **1991**, *94*, 5360.

(32) Winter, R.; Hua, D. W.; Song, X.; Mantulin, W.; Jonas, J. *J. Phys. Chem.* **1990**, *94*, 2706.

(33) (a) Itho, K.; Honda, K. *Chem. Phys. Lett.* **1982**, *87*, 213. (b) Vogel, M.; Rettig, W.; Sens, R.; Drexhage, K. H. *Chem. Phys. Lett.* **1988**, *147*, 461

(34) (a) Vieria-Ferreira, L. F.; Cabral, P. V.; Almeida, P.; Oliveira, A. S.; Bothelo do Rego, A. M. *Macromolecules* **1998**, *31*, 3936 and references therein. (b) Slyadneva, O. N.; Slyadnev, M. N.; Tsukanova, V. M.; Inoue, T.; Harata, A.; Ogawa, T. *Langmuir* **1999**, *15*, 8651.

(35) (a) Nakashima, N.; Yoshihara, K.; Willig, F. *J. Chem. Phys.* **1980**, *73*, 3553. (b) Liang, Y.; Moy, P. F.; Poole, J. A.; Ponte Goncalves, A. M. *J. Phys. Chem.* **1984**, *88*, 2451. (c) Nasr, C.; Liu, D.; Hotchandani, S.; Kramat, P. V. *J. Phys. Chem.* **1996**, *100*, 11054. (d) Ballet, P.; Van der Auweraer, M.; De Schyver, F. C.; Lemmtyinen, H.; Vuorimaa, E. *J. Phys. Chem.* **1996**, *100*, 13701.

(36) (a) López-Arbeloa, F.; Martínez-Martínez, V.; Bañuelos-Prieto, J.; López-Arbeloa, I. *Langmuir* **2002**, *18*, 2658 and references therein. (b) Bojarski, P.; Matczuk, A.; Bojarski, C.; Kawski, A.; Kuklinski, B.; Zurkowska, G.; Diehl, H. *Chem. Phys.* **1996**, *210*, 485.

(37) Karstane, T.; Kobe, K. *J. Phys. Chem.* **1980**, *84*, 1871.

(38) del Monte, F.; Mackenzie, J. D.; Levy, D. *Langmuir* **2000**, *16*, 7377.

(39) Cornil, J.; dos Santos, D. A.; Crispin, X.; Silbey, R.; Bredas, J. L. *J. Am. Chem. Soc.* **1998**, *120*, 1289−1299.

(40) Horn, D.; Rieger, J. *Angew. Chem., Int. Ed.* **2001**, *40*, 4330.

(41) Lannibois, H.; Hasmy, A.; Botet, R.; Chariol, O. A.; Cabane, B. *J. Phys. II* **1997**, *7*, 319.